Reduction and archiving of multiwavelength, polarized-intensity debris-disk observations with the Gemini planet imager

Crotts, Katie A.; Esposito, Thomas M.; Matthews, Brenda C.; Duchêne, Gaspard; Chen, Christine H.; Hom, Justin; Kalas, Paul; Lewis, Briley L.; Metchev, Stanimir; Millar-Blanchaer, Maxwell; Padgett, Deborah; Perrin, Marshall; Ren, Bin

Publisher's version / Version de l'éditeur:

https://doi.org/10.3847/1538-4365/ad90a4

The Astrophysical Journal Supplement Series, 276, 1, 2024-12-26

The Astrophysical Journal Supplement Series, 276:14 (6pp), 2025 January https://doi.org/10.3847/1538-4365/ad90a4

Reduction and Archiving of Multiwavelength, Polarized-intensity Debris-disk Observations with the Gemini Planet Imager

Katie A. Crotts[1], Thomas M. Esposito[2,3], Brenda C. Matthews[1,4], Gaspard Duchêne[2,5], Christine H. Chen[6], Justin Hom[7], Paul Kalas[2,3,8], Briley L. Lewis[9], Stanimir Metchev[10], Maxwell Millar-Blanchaer[11], Deborah Padgett[12], Marshall Perrin[6], and Bin Ren[13]

[1] Physics & Astronomy Department, University of Victoria, 3800 Finnerty Road, Victoria, BC V8P 5C2, Canada
[2] Astronomy Department, University of California, Berkeley, CA 94720, USA
[3] SETI Institute, Carl Sagan Center, 339 Bernardo Avenue, Mountain View, CA 94043, USA
[4] Herzberg Astronomy and Astrophysics, National Research Council of Canada, 5071 West Saanich Road, Victoria, BC V9E 2E7, Canada
[5] Université Grenoble Alpes/CNRS, Institut de Planétologie et d'Astrophysique de Grenoble, 38000 Grenoble, France
[6] Space Telescope Science Institute (STScI), 3700 San Martin Drive, Baltimore, MD 21218, USA
[7] Steward Observatory and Department of Astronomy, University of Arizona, Tucson, AZ 85721, USA
[8] Institute of Astrophysics, FORTH, GR-71110 Heraklion, Greece
[9] Department of Physics and Astronomy, 430 Portola Plaza, University of California, Los Angeles, CA 90095, USA
[10] Department of Physics & Astronomy, Western University, London, ON N6A 3K7, Canada
[11] Department of Physics, University of California, Santa Barbara, CA 93106, USA
[12] Jet Propulsion Laboratory, California Institute of Technology, 4800 Oak Grove Drive, Pasadena, CA 91109, USA
[13] Université Côte d'Azur, Observatoire de la Côte d'Azur, CNRS, Laboratoire Lagrange, Bd de l'Observatoire, CS 34229, 06304 Nice cedex 4, France
Received 2024 August 1; revised 2024 November 4; accepted 2024 November 4; published 2024 December 26

Abstract

The Gemini Planet Imager (GPI), an extreme adaptive optics instrument on Gemini South, has been pivotal in the advancement of the debris-disk field. Over the past decade, GPI has observed tens of debris disks at near-infrared wavelengths in both polarized and total intensity as a part of several direct-imaging surveys. Here we discuss the uniform reductions of the *J*-, *H*- and *K*1-band GPI observations, specifically in polarized intensity. This includes 24 debris-disk observations in the *H* band, 10 debris-disks observations in the *J* band and 11 disk observations in the *K*1 band. Additionally, all three reduced data sets have been archived on the digital platform, CANFAR, so that they are available for public use. The purpose of this work is to provide the necessary steps for one to carry out their own data reductions if desired, as well as to create a space where these uniformly reduced data are easily accessible for future analysis and research.

Unified Astronomy Thesaurus concepts: Debris disks (363); Near infrared astronomy (1093); Astronomy data reduction (1861); Astronomy data acquisition (1860)

1. Introduction

In recent years, high-contrast imaging has drastically improved in both resolution and sensitivity, which has allowed us to spatially resolve more debris disks than ever before. The Gemini Planet Imager (GPI), an extreme adaptive optics instrument located on Gemini South from 2013 to 2022, is one of the most recent ground-based instruments optimized for exoplanet detection (B. Macintosh et al. 2014), but has also produced a wealth of imaging data on debris disks. For example, as part of the Gemini Planet Imager Exoplanet Survey (GPIES), a campaign dedicated to the search of giant planets around ∼600 nearby stars (B. Macintosh et al. 2018), 26 debris disks were imaged in polarized and/or total intensity, where two of these disks were imaged in scattered light for the first time (T. M. Esposito et al. 2020).

While GPIES focused solely on *H*-band observations, other GPI surveys have additionally targeted these disks in other near-infrared wavelengths. This includes an awarded Large and Long Program (PID GS-2018A-LP-6; PI: C. Chen), where roughly half of the debris disks observed through GPIES were also observed in the *J* and *K*1 bands. Both the polarized- and total-intensity *H*-band data were first uniformly reduced and presented as a group in T. M. Esposito et al. (2020), while the polarized-intensity *J*- and *K*1-band data were uniformly reduced and presented as a group in K. A. Crotts et al. (2024). However, despite these data sets being uniformly reduced and published, they have not been made publicly accessible, limiting the usefulness of these data sets for further studies by the community.

In this paper, we discuss the uniform reductions of the *J*, *H*, and *K*1 data in polarized intensity presented in T. M. Esposito et al. (2020) and K. A. Crotts et al. (2024). We focus primarily on the polarized-intensity observations as one-third of the disks in our sample are not recovered in total intensity due to an unfavorable viewing geometry (such as a low inclination) and/or a low signal-to-noise ratio (SNR). Additionally, all three polarized data sets were uniformly reduced using a similar procedure optimized to reduce the amount of noise in each image and recover as much disk signal as possible. Further details about the reduction process can be found in Section 2. In addition to the uniform reductions, we have archived all three data sets (GPI *J*, *H*, and *K*1 polarized intensity) on the publicly accessible website CANFAR, with the intention of making our reduced data easily obtainable for future research. Further details on this will be discussed in Section 3.

2. Observations and Data Reduction

The observations of the *J* ($\lambda_c = 1.25\ \mu$m), *H* ($\lambda_c = 1.65\ \mu$m), and *K*1 ($\lambda_c = 2.05\ \mu$m) data were executed over the span of

Table 1
Summary of Observations

Name	Band	Date	Inner Radius and Outer Radius	Frame ID/Total Number Removed
AU Mic[a]	*H*	140515	10, 13	367–369/3
β Pic[a]	*H*	131212	7, 13	189–194, 223/7
CE Ant	*H*	180405	13, 15	N/A
HD 30447	*H*	160922	13, 15	N/A
HD 32297	*J*	151206	10, 13	N/A
...	*H*	141218	1, 3	165–166/2
...	*K*1	161118	7, 11	336–339/4
HD 35841	*J*	180127	7, 11	46–59/14
...	*H*	160318	2, 7	14–21/8
...	*K*1	171228	7, 11	36–38 and 88–91/7
HD 61005[a]	*J*	151201	7, 11	N/A
...	*H*	140324	8, 11	N/A
...	*K*1	180126	7, 11	127–131/5
HD 106906	*J*	160326	2, 7	161/1
...	*H*	150701	10, 13	71/1
...	*K*1	160328	2, 7	203–206/4
HD 110058	*J*	180126	10, 13	N/A
...	*H*	160319	8, 11	N/A
...	*K*1	170420	7, 11	136–139/4
HD 111161	*H*	180310	13, 17	203/1
HD 111520	*J*	160326	–1, 25	219–224/6
...	*H*	160318	10, 13	248–250/3
...	*K*1	160328	10, 13	248–252/5
HD 114082	*H*	170807	10, 15	44–51/8
...	*K*1	170420	7, 11	173–176/4
HD 115600	*J*	180128	10, 13	N/A
...	*H*	150703	13, 15	N/A
...	*K*1	180127	7, 11	225–227 and 273–276/7
HD 117214	*H*	180311	13, 15	N/A
HD 129590	*H*	170809	8, 11	9–10/2
...	*K*1	170421	7, 11	125–128/4
HD 131835	*H*	150501	8, 11	N/A
HD 143675	*H*	180408	10, 13	N/A
HD 145560	*H*	180812	8, 11	N/A
HD 146897	*J*	160327	7, 11	N/A
...	*H*	160321	7, 13	99/1
...	*K*1	180709	7, 11	158–159/2
HD 156623	*H*	190427	13, 15	N/A
HD 157587	*J*	160326	7, 11	363/1
...	*H*	150829	7, 13	N/A
...	*K*1	160327	7, 11	N/A
HD 191089	*J*	170701	7, 11	145–151/7
...	*H*	150901	10, 13	313/1
HR 4796 A[a]	*H*	131212	8, 11	N/A
HR 7012	*H*	180921	13, 15	3/1

Notes. The date is in the format YYMMDD. The Inner Radius and Outer Radius refer to the radius in pixels used to measure the mean stellar polarization behind the FPM. The last column states which data frames (identified by their ID) were removed due to poor alignment of the star behind the coronagraph, as well as the total number of frames removed.
[a] *H*-band observations taken during GPI commissioning.

several years, from 2013 December through 2019 April as part of commissioning, GPIES, and the Debris Disk Large and Long Program. This included 24 debris disks in the *H* band, 10 disks observed in the *J* band, and 11 disks observed in the *K*1 band, listed in Table 1. All data were taken in polarimetric ("J-Pol," "H-Pol," and "K1-Pol") mode with a pixel scale of 14.161 ± 0.021 mas per lenslet (R. J. De Rosa et al. 2020) and a field of view of $2\farcs8$ by $2\farcs8$. In polarimetric mode, a rotating half-wave plate is utilized and positioned at angles [0°.0, 22°.5, 45°.0, 67°.5] for each observing sequence to measure the different linear polarization states (i.e., Stokes parameters $\mathcal{I}$, $\mathcal{Q}$, and $\mathcal{U}$), while a polarizing Wollaston prism beam splitter is then used to divide the light into two orthogonal polarization states. The focal plane mask (FPM) differs in size between all three bands, where the FPM has a radius of $0\farcs09$ in the *J* band, $0\farcs12$ in the *H* band, and $0\farcs15$ in the *K*1 band. Further details about the observations and systems themselves can be found in T. M. Esposito et al. (2020) and K. A. Crotts et al. (2024).

All data were reduced using the GPI Data Reduction Pipeline[14] (DRP; M. D. Perrin et al. 2014, and references therein). The data reduction process for these data sets is already described at length in T. M. Esposito et al. (2020) and K. A. Crotts et al. (2024), however, for thoroughness, we briefly resummarize them here with more emphasis on the overall steps of the reduction process rather than the technical details. For a more comprehensive overview of the DRP and technical details of the reduction process, we direct the interested reader to M. D. Perrin et al. (2014, 2016) and J. J. Wang et al. (2018). Our main goal of stating the reduction process is to give other researchers the information for conducting their own data reduction of the data if required.

To start, the raw data frames are retrieved[15] and are visually inspected for quality control. For example, several data frames, typically at the beginning or end of the observing sequence, often have poor alignment of the star behind the coronagraph, and are therefore removed. Once bad data frames are removed, the raw date are then processed through the reduction pipeline, via the "Basic Polarization Sequence (From Raw Data)," to create three-dimensional data cubes containing spatial information (x, y) and the orthogonal polarization. In this first reduction step, the raw data are dark subtracted, "destriped" (striped artifacts produced by correlated detector noise and vibration-induced microphonics), bad-pixel corrected, flat-field corrected, and distortion corrected. Additionally, the position of the star is measured using fiducial satellite spots, i.e., first-order diffraction spots of the starlight (J. J. Wang et al. 2014), which are used in later steps for photometric calibration. Once the raw data are processed into 3D data cubes, the data cubes are again visually inspected to ensure no bad calibration files were used. Additionally, the location of the star (measured using the satellite spots) is double checked through searching "PSFCENTX" and "PSFCENTY" in the headers for each data cube to identify any additional frames where the star was not centered correctly behind the coronagraph. The frames that were removed for each data set are stated in Table 1 under "Frames Removed."

Once the raw data are processed into data cubes and all bad frames are identified, the remaining data cubes are further reduced into a single azimuthal Stokes image using the "Basic Polarization Sequence (From podc cubes)." Through this sequence, all data cubes are accumulated, further cleaned, and are smoothed using a Gaussian kernel with an FWHM of

[14] Instructions for downloading and installing the GPI DRP can be found at https://github.com/geminiplanetimager/gpi_pipeline. Documentation for using the DRP can be found at https://docs.planetimager.org/pipeline/index.html.
[15] Raw data for each disk, except for those taken during commissioning, can be obtained from https://archive.gemini.edu/searchform.

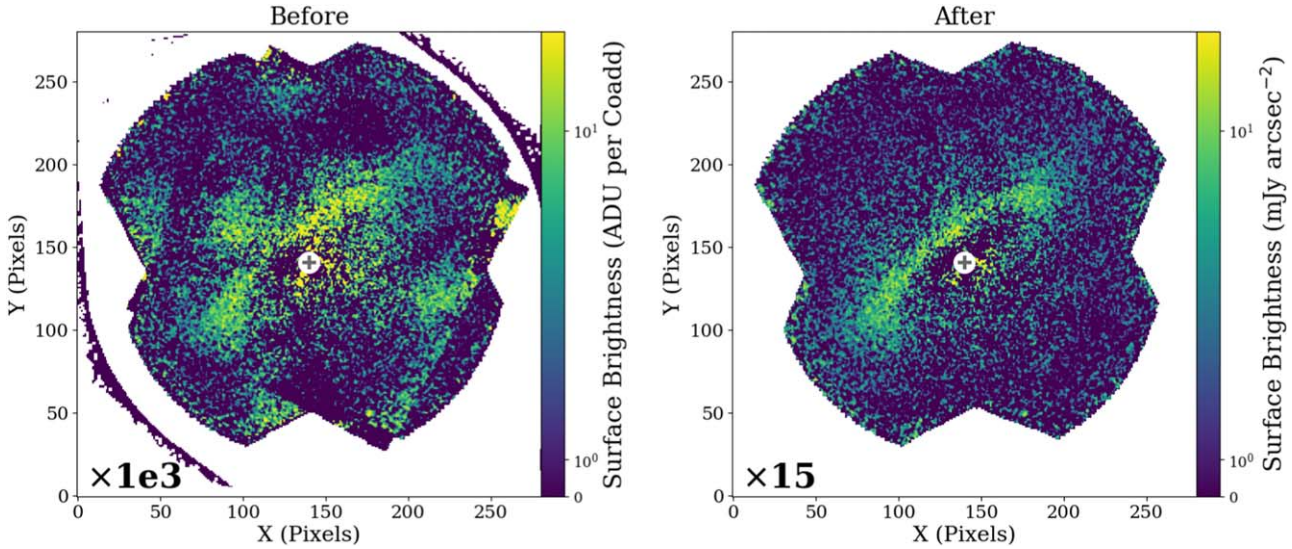

Figure 1. Example transformation between the autoreduced data (left) and our uniformly reduced data published in K. A. Crotts et al. (2024) (right) for the HD 157587 disk in the *J* band. Both data are scaled by the number in the lower-left corner. The circles represent the size of the FPM ($0\farcs09$), and the crosses represent the location of the star.

1 pixel. In the next step, the mean stellar polarization is subtracted from the image, which is done by measuring the polarization in an annulus near the FPM (M. A. Millar-Blanchaer et al. 2016). The default settings for the annulus in this step are an inner radius of –1 pixel and an outer radius of 25 pixels from the star, however, changing the inner and outer radius can lead to a much cleaner final image. We find that a 2–5 pixel wide annulus centered between 2 and 15 pixels from the star was the most effective at removing the mean stellar polarization. The inner and outer radius of the annulus used for each data set can be found in Table 1. It should be noted that the determination of the best annulus location and size was done merely by eye. Once the mean stellar polarization is removed, the image is rotated so that north is up and combined into a single cube with Stokes parameters $[\mathcal{I}, \mathcal{Q}, \mathcal{U}, \mathcal{V}]$, where $\mathcal{I}$ is the total intensity component, $\mathcal{Q}$ and $\mathcal{U}$ are the linear polarization components, and $\mathcal{V}$ is the circular polarization component. The combined image is then transformed to azimuthal Stokes vectors $\mathcal{Q}_\phi$ and $\mathcal{U}_\phi$ defined as

$$\begin{aligned} \mathcal{Q}_\phi &= -\mathcal{Q}\cos 2\phi - \mathcal{U}\sin 2\phi \\ \mathcal{U}_\phi &= +\mathcal{Q}\sin 2\phi - \mathcal{U}\cos 2\phi \end{aligned} \quad (1)$$

where ϕ is the azimuthal angle between each pixel and the star measured counterclockwise from $-\pi$ to π (H. M. Schmid et al. 2006; M. A. Millar-Blanchaer et al. 2016). As a result, $\mathcal{Q}_\phi$ contains the linearly polarized disk signal and $\mathcal{U}_\phi$ (which is aligned $\pm 45°$ from $\mathcal{Q}_\phi$) should only contain noise assuming an optically thin debris disk causing single scattering. Finally, the image is converted from units of ADU per coadd to real units of Jy arcsec^{-2} using the satellite spot measurements of the stellar flux.

While the reduction process would typically stop here, we conduct one extra step, described in both T. M. Esposito et al. (2020) and K. A. Crotts et al. (2024). To summarize, we attempt to remove a quadrupole-like noise pattern that is commonly seen in GPI polarized-intensity data due to imperfect subtraction of the instrumental polarization. The intensity and orientation of this pattern is measured using the $\mathcal{U}_\phi$ image via the equation $B = B_0 \mathcal{I}_r \sin 2(\theta + \theta_0)$, $\mathcal{I}_r$ being the azimuthally averaged total intensity as a function of radius from the star. The function is then fit by varying the scaling factor B_0 and offset angle θ_0. Once the residuals are minimized, the best-fitting function is subtracted from the $\mathcal{U}_\phi$ image, rotated by 45°, then subtracted from the $\mathcal{Q}_\phi$ image.

At this stage, the data have been effectively cleaned as much as possible. As an example, Figure 1 shows our new reduction of the HD 157587 disk in the *J* band compared to the initial autoreduction (which is not flux calibrated), highlighting the major improvement in data quality. To quantify this improvement, we compare the SNR along the disk's major axis for both reductions. To estimate the SNR, we divide noise maps from the Q_ϕ data. These noise maps are generated from the U_ϕ data by measuring the standard deviation at each radius in 1 pixel wide stellocentric annuli. We find the autoreduced data to have an average SNR of 1.4 per pixel along the major axis, while in our reduction, the average SNR increases to 2.0 per pixel, signifying a ∼35%–40% improvement in SNR. The final data reductions for all the disks in the *H*, *J*, and *K*1 bands can be seen in Figures 2 and 3. In all cases, the noise was significantly reduced, and the disk itself was better recovered. For only a small handful of observations does a high amount of noise persist, such as the case for AU Mic in the *H* band and the HD 61005 observations in both the *J* and *K*1 bands. While we are unable to significantly reduce the noise in these data sets, given that they are very low SNR observations to begin with, the disk signal is still better recovered compared to the autoreduced data.

3. Data Archive

Now that all three data sets are uniformly reduced in an optimized manner, the data can be stored publicly for future analysis and research by any member of the astronomy community. In addition to being full reductions, these data also contain important and useful details in their headers including information about the observation and observing conditions, reduction steps, parameters, and calibrations files used, etc. We choose to store these data on the the Canadian

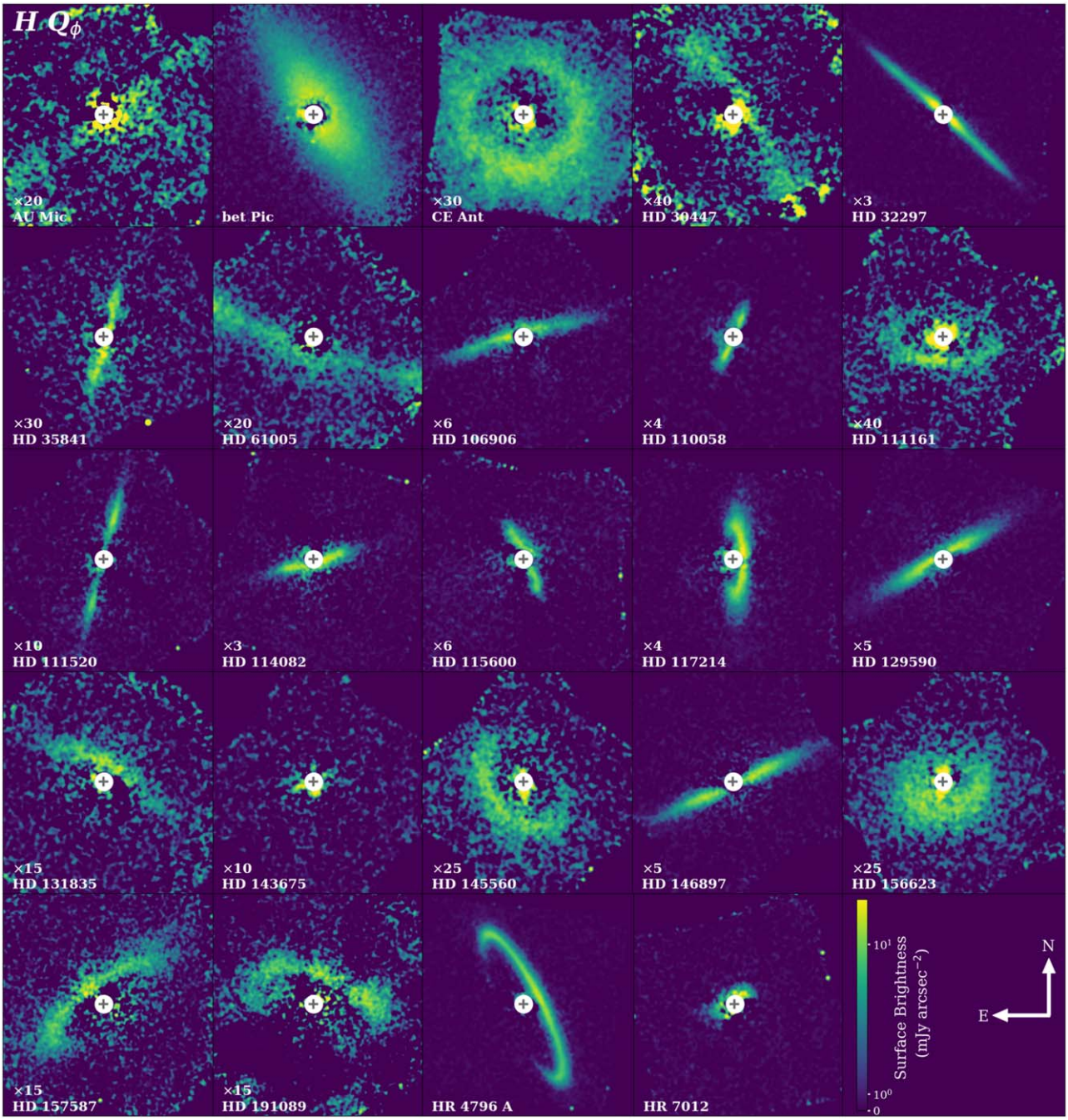

Figure 2. Final HQ_ϕ reductions presented in T. M. Esposito et al. (2020). The circles represent the size of the FPM in the H band ($0\farcs12$), and the crosses represent the location of the star. Similar to Figure 5 in T. M. Esposito et al. (2020), the data are scaled in units of mJy arcsec^{-2} by the numbers in the lower-left corner in order to have similar brightness. Additionally, the disk surface brightness is linear from 0 to 1, with a log scale from 1 to 20 mJy arcsec^{-2}. For all data, east is left and north is up.

Advanced Network for Astronomical Research platform (CANFAR). CANFAR is a consortium dedicated to serving computing and data intensive resources to members of universities and centers engaged in astronomical research, and can be used to store and manage data via a VOSpace. Through their storage system, CANFAR also provides the Data Publication Service which allows one to connect a Digital Object Identifier (DOI) to data sets presented in a research paper. Therefore, by storing these data sets on CANFAR, we can attach a DOI that will make the data easily and permanently searchable. Following this procedure, the data can be obtained through doi:10.11570/24.0089. The data stored on CANFAR are categorized by filter (J, H, and $K1$) and are labeled by filter and name of the object for easy finding. A "README" file can also be found with extra information regarding citation requirements and the DRP recipe template mentioned in Section 2 with the listed steps. To summarize, we have provided a permanent location to store our best reductions of the polarized-intensity, multiwavelength, GPI debris-disk observations, alongside additional resources to help summarize the data reduction process. Future work may involve uniform reductions of the multiwavelength GPI debris-disk data in total

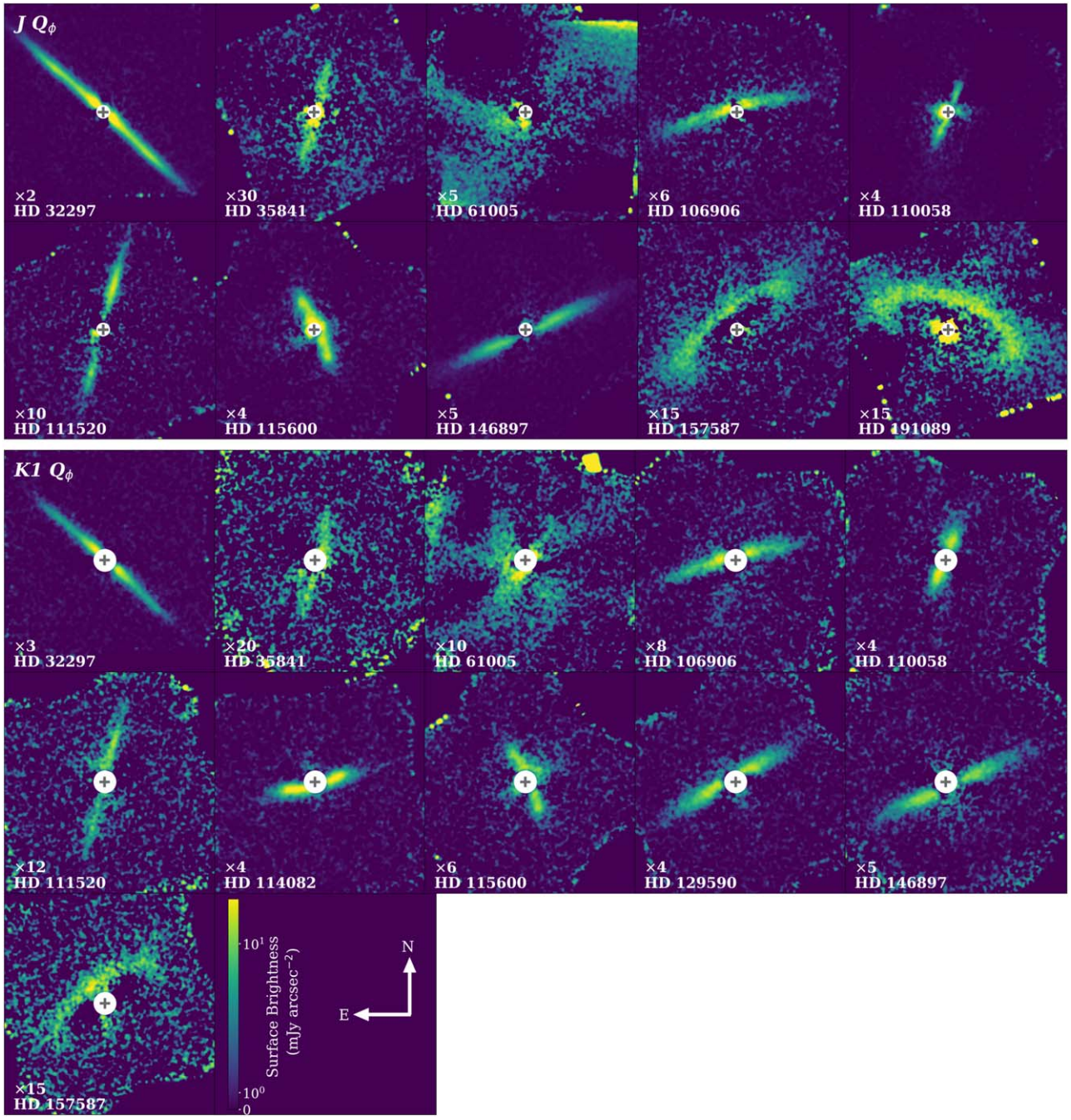

Figure 3. Final *J*- (top) and *K*1-band (bottom) $\mathcal{Q}_\phi$ reductions presented in K. A. Crotts et al. (2024). The circles represent the size of the FPM in the *J* and *K*1 bands ($0\farcs09$ and $0\farcs15$, respectively), and the crosses represent the location of the star. Similar to Figure 2 and Figure 5 in T. M. Esposito et al. (2020), the data are scaled in units of mJy arcsec^{-2} by the numbers in the lower-left corner in order to have similar brightness. Additionally, the disk surface brightness is linear from 0 to 1, with a log scale from 1 to 20 mJy arcsec^{-2}. For all data, east is left and north is up.

intensity (see T. M. Esposito et al. 2020 for the total intensity reductions in the *H* band), which can then be similarly archived.

4. Conclusions

In this paper we discuss the data reduction steps of the GPI *J*, *H*, and *K*1 polarized-intensity observations, first presented as a group in T. M. Esposito et al. (2020) and K. A. Crotts et al. (2024). The purpose of discussing the data reduction steps is to provide other researchers with the tools to conduct their own data reduction if required. We ensure the best quality reductions by removing frames with poor alignment of the star behind the coronagraph, double checking the quality of the calibration files, adjusting the annulus size and location to efficiently remove the mean stellar polarization, as well as removing a quadrupole-like pattern in each final image. In addition to the uniform data reductions, we also provide a public space on CANFAR to store these GPI data sets with a permanent DOI. The main purpose for the storage on CANFAR is to provide other members of the astronomy community the ability to easily obtain our well-reduced data for future research and analysis.

Acknowledgments

We wish to thank the anonymous referee for constructive comments that improved the manuscript. This work is based on observations obtained at the Gemini Observatory, which is operated by the Association of Universities for Research in Astronomy, Inc. (AURA), under a cooperative agreement with the National Science Foundation (NSF) on behalf of the Gemini partnership: the NSF (United States), the National Research Council (Canada), CONICYT (Chile), Ministerio de Ciencia, Tecnología e Innovación Productiva (Argentina), and Ministério da Ciência, Tecnologia e Inovação (Brazil). This work made use of data from the European Space Agency mission Gaia (https://www.cosmos.esa.int/gaia), processed by the Gaia Data Processing and Analysis Consortium (DPAC, https://www.cosmos.esa.int/web/gaia/dpac/consortium). Funding for the DPAC has been provided by national institutions, in particular the institutions participating in the Gaia Multilateral Agreement. This research made use of the SIMBAD and VizieR databases, operated at CDS, Strasbourg, France. We thank support from NSF AST-1518332, NASA NNX15AC89G and NNX15AD95G/NEXSS. Portions of this work were also performed under the auspices of the U.S. Department of Energy by Lawrence Livermore National Laboratory under contract DE-AC52-07NA27344. K.A.C. and B.C.M. acknowledge a Discovery Grant from the Natural Science and Engineering Research Council of Canada.

Facility: Gemini:South

Software: Gemini Planet Imager Pipeline (GPI instrument collaboration 2014; M. D. Perrin et al. 2014) matplotlib (J. D. Hunter 2007; M. Droettboom et al. 2017), iPython (F. Perez & B. E. Granger 2007), Astropy (Astropy Collaboration et al. 2013, 2018, 2022), NumPy (C. R. Harris et al. 2020; https://numpy.org), SciPy (P. Virtanen et al. 2020; http://www.scipy.org/).

ORCID iDs

Katie A. Crotts https://orcid.org/0000-0003-4909-256X
Thomas M. Esposito https://orcid.org/0000-0002-0792-3719
Brenda C. Matthews https://orcid.org/0000-0003-3017-9577
Gaspard Duchêne https://orcid.org/0000-0002-5092-6464
Christine H. Chen https://orcid.org/0000-0002-8382-0447
Justin Hom https://orcid.org/0000-0001-9994-2142
Paul Kalas https://orcid.org/0000-0002-6221-5360
Briley L. Lewis https://orcid.org/0000-0002-8984-4319
Stanimir Metchev https://orcid.org/0000-0003-3050-8203
Maxwell Millar-Blanchaer https://orcid.org/0000-0001-6205-9233
Deborah Padgett https://orcid.org/0000-0001-5334-5107
Marshall Perrin https://orcid.org/0000-0002-3191-8151
Bin Ren https://orcid.org/0000-0003-1698-9696

References

Astropy Collaboration, Price-Whelan, A. M., Lim, P. L., et al. 2022, ApJ, 935, 167
Astropy Collaboration, Price-Whelan, A. M., Sipőcz, B. M., et al. 2018, AJ, 156, 123
Astropy Collaboration, Robitaille, T. P., Tollerud, E. J., et al. 2013, A&A, 558, A33
Crotts, K. A., Matthews, B. C., Duchêne, G., et al. 2024, ApJ, 961, 245
De Rosa, R. J., Nguyen, M. M., Chilcote, J., et al. 2020, JATIS, 6, 015006
Droettboom, M., Caswell, T. A., Hunter, J., et al. 2017, matplotlib/matplotlib v2.0.2, Zenodo, doi:10.5281/zenodo.573577
Esposito, T. M., Kalas, P., Fitzgerald, M. P., et al. 2020, AJ, 160, 24
GPI instrument collaboration, 2014 GPI Pipeline: Gemini Planet Imager Data Pipeline, Astrophysics Source Code Library, ascl:1411.018
Harris, C. R., Millman, K. J., van der Walt, S. J., et al. 2020, Natur, 585, 357
Hunter, J. D. 2007, CSE, 9, 90
Macintosh, B., Chilcote, J. K., Bailey, V. P., et al. 2018, Proc. SPIE, 10703, 107 030K
Macintosh, B., Graham, J. R., Ingraham, P., et al. 2014, PNAS, 111, 12661
Millar-Blanchaer, M. A., Perrin, M. D., Hung, L.-W., et al. 2016, Proc. SPIE, 9908, 990836
Perez, F., & Granger, B. E. 2007, CSE, 9, 21
Perrin, M. D., Ingraham, P., Follette, K. B., et al. 2016, Proc. SPIE, 9908, 990837
Perrin, M. D., Maire, J., Ingraham, P., et al. 2014, Proc. SPIE, 9147, 91473J
Schmid, H. M., Joos, F., & Tschan, D. 2006, A&A, 452, 657
Virtanen, P., Gommers, R., Oliphant, T. E., et al. 2020, NatMe, 17, 261
Wang, J. J., Perrin, M. D., Savransky, D., et al. 2018, JATIS, 4, 018002
Wang, J. J., Rajan, A., Graham, J. R., et al. 2014, Proc. SPIE, 9147, 914755